Research Article Vol. 30, No. 4 / 14 Feb 2022 / Optics Express 5329
Optics EXPRESS

Study of deterministic surface micro-texture generation in ultra-precision grinding considering wheel oscillation

SHANSHAN CHEN,[1,2,3] SHUMING YANG,[1,6] ZHIRONG LIAO,[3,7] CHI FAI CHEUNG,[4] ZHUANGDE JIANG,[1] AND FEIHU ZHANG[5]

[1]State Key Laboratory for Manufacturing Systems Engineering, Xi'an Jiaotong University, 28 Xianning West Road, Xi'an, Shaanxi 710049, China
[2]Research Institute of Xi'an Jiaotong University, Zhejiang, China
[3]Faculty of Engineering, University of Nottingham, NG7 2RD, UK
[4]State Key Laboratory of Ultraprecision Machining Technology, The Hong Kong Polytechnic University, Hung Hom, Kowloon 999077, Hong Kong
[5]School of Mechatronics Engineering, Harbin Institute of Technology, Harbin 150001, China
[6]shuming.yang@mail.xjtu.edu.cn
[7]zhirong.liao@nottingham.ac.uk

Abstract: Ultra-precision grinding is crucial for manufacturing high-end optics and molds, while the unbalanced wheel vibration is inevitable and becomes even more critical in surface generation, which resulted in undesired waviness and micro-texture on the ground surface. In this paper, to understand and control the micro-texture generation, a theoretical model has been developed to predict the deterministic surface micro-texture generation resulted from unbalanced tool vibration in ultra-precision grinding, in which the overlap trajectories of grinding wheel with an arc cutting edge were analyzed and calculated. The simulation work was performed and a double phase mechanism involved in deterministic textural pattern and structure has been revealed. Both theoretical and experimental results proved that phase shift is an important factor to determine micro-texture evolution in the ultra-precision grinding process. On this basis, a novel tool path strategy has been proposed to fabricate deterministic micro-structure by coordinating oscillation motion of the grinding wheel and phase shift control, in which a rhombus-shaped micro-structure array can be generated. A small adjustment for the phase shift was conducted and it was found that the more complex micro-texture with different textural patterns and micro-structure can be machined. The results indicated that the phase control for the tool path planning is an effective method to fabricate flexible and tunable micro-texture surfaces in ultra-precision grinding.

1. Introduction

High precision optical elements with complex structure have driven the need for more deterministic machining process, which is the key procedure to control their surface quality and form deviations [1–4]. For high precision optical components, most of them are made of hard and brittle materials, such as Silicon Carbide (SiC), Germanium (Ge), Tungsten Carbide (WC) and Glass. Ultra-precision grinding is widely used to achieve the high lever form accuracy and surface finish for the optical elements [3–5]. However, in the grinding process, the surface generation is closely related to the static and dynamic characteristics of the machine tool. In particular, the vibration of the grinding wheel leads to the excess movement of the grinding wheel relative to the workpiece surface, which degrades the quality of the machined surface and has an important impact on the

#452751 https://doi.org/10.1364/OE.452751
Journal © 2022 Received 2 Jan 2022; revised 27 Jan 2022; accepted 27 Jan 2022; published 3 Feb 2022

Optics EXPRESS

surface error formation [6]. There are two main vibration types in grinding: forced vibration and self-excited vibration. Forced vibration mainly comes from the eccentric installation of grinding wheel spindle, runout, dressing error, errors in grinding wheel manufacturing process and uneven wear in machining process [7–9]. Self-excited vibration is mainly caused by the alternating grinding force of the grinding system itself. Many monitoring and analysis of the grinding process show that the wheel unbalance is the main cause of tool vibration (forced vibration) [10–12]. The unbalanced vibration is difficult to eliminate completely even if fine dressing and accurate dynamic balance are conducted, whereby a series of vibration marks can still be generated on the ground surface [12]. For the unbalanced vibration, the tool oscillates at the wheel spindle rotation frequency. Therefore, the micro-waviness structure (wavelength and frequency) is deterministic and closely related to the speed ratio of the grinding wheel to workpiece.

The waviness has a direct influence on the scallop height of the ground surface profile, and it would deteriorate the surface quality and optical performance [13], which has attracted wide attention from academics and industry. Zhang [14] et al. evaluated dynamic characteristics of the grinding wheel based on kinematics analysis and proposed a method to calculate the influence of cutting factors on the tool vibration. Badger [15] et al. investigated the effect of wheel eccentricity on surface topography and predict waviness and established the relationship between the scallop height and waviness under different grinding conditions. Chen [16] et al. established the distribution of the lowest grinding point by considering the wheel vibration in grinding of the aspheric surface and it is found that the uniform distribution of grinding point is beneficial to reduce vibration marks. In fact, the deterministic waviness marks have a close relationship with the phase shift of tool vibration, in which the fractional part of the speed ratio of the grinding wheel to the workpiece determines the mark geometry [17]. Pan [18] et al. developed the theoretical model for surface waviness generation by considering the interference-overlapping effect of wheel cutting profile in the feed direction. It was shown that wave shift plays a critical role in the reduction of waviness error in the grinding and non-integer speed ratio is useful to improve the surface uniformity and quality. Chen [19] et al. investigated the correction between the phase shift and spiral vibration marks and proposed that the surface roughness can be improved remarkably with the middle shift in the ultra-precision grinding. Those research work indicated that phase shift posed a significant effect on both deterministic waviness and surface roughness. In grinding of the curved surface, the waviness is still the major error for surface generation. Chen [20] et.al established the relationship between waviness spatial amplitude and surface curvature and it is found that waviness can result in nonuniform surface topography in grinding of the curved surfaces. Wang [21] et.al analyzed the influence of operation parameters on the evolution mechanism of vibration marks in terms of residual height, waviness period, and inclination angle in the machining of spherical surfaces. The results showed that the integer speed ratio mainly determines the distribution density of grinding points, while the fractional part of the ratio, mainly affects the meridional pitch.

Although the passive vibration errors can be inevitably induced in the ultra-precision machining and deteriorate the surface quality, the active vibration can also be beneficial to assist the machining process. Recently ultrasonic vibration-assisted technology is increasingly applied to various machining processes, such as single point diamond turning [22–24], micro-milling [25,26], and grinding [27–29]. The vibration-assisted turning [30] and milling [31] are mainly used for generating special deterministic micro/nano-texture, in which the cutting tool or workpiece is applied a small and high frequency vibration [32]. For vibration-assisted grinding, which mainly aims to improve the machinability of hard and brittle materials, which is beneficial to cut in a ductile material removal mode and to reduce the crack generation [33]. In the vibration assisted grinding, it has been proven that high frequency vibration can improve surface roughness and reduce defects not only in machining flat surface [34], but also curved surface [35] and even

Optics EXPRESS

micro-structured surface [36]. The ultrasonic vibration can increase the interaction overlap ratio of the wheel trajectory within the cutting regime to improve surface quality as well as surface integrity. For the vibration-assisted grinding, the cutting trajectory of abrasive grain is established by both grinding operation parameters and vibration variables, in which the superposition effect of those traces can lead to the final "staggered surface texture" generation [37]. It has been revealed that the chip scale and grinding force can be reduced significantly under the high frequency vibration, which can eventually improve the ground surface roughness and decrease subsurface damage [38]. However, the vibration textures are not deterministic due to the random features of abrasive grains, which are also generated in a mode of random distribution [39–41].

Ultra-precision grinding has an outstanding capability for machining of various hard and brittle materials, which plays a critical role in fabricating optical elements [42,43]. At present, the macro-waviness related to the grinding wheel vibration (i.e. passive vibration errors) and the micro-texture related to the oscillation of abrasive grains (i.e. vibration-assisted grinding) have been investigated extensively. It mainly focused on the surface waviness generation and surface roughness prediction. However, little attention has been focused on the deterministic micro-texture generation resulted from the unbalance vibration of grinding wheel.

In our previous studies, the primary phase shift mechanism for the surface waviness generation has been studied and the evolution mechanism of surface waviness under different phase shifts has been revealed under the unbalanced wheel vibration [19]. However, it is not clear that the role of the second phase shift involved in ultra-precision grinding and generation mechanism of deterministic surface micro-texture. In this paper, a model based on the overlapping effect of wheel cutting edge in the successive tool paths was developed in ultra-precision grinding, in which the cutting profile intersection of grinding wheel between neighboring tool traces was first deduced by considering the phase shift effect. Next, the impacts of the second phase shift on the waviness generation and evolution of deterministic micro-texture were studied. Finally, a novel tool path planning method was proposed to fabricate micro-structure surface based on the phase shift control.

2. Theoretical modelling of surface micro-texture generation in ultra-precision grinding

In ultra-precision grinding, fine feed speed is usually adopted to achieve a good surface finish, which was beneficial to intensify the adjacent cutting tool profile interference so as to reduce residual profile height. Hence, even the micro-vibration of the grinding wheel can pose a detrimental effect on machined surface quality. In the occurrence of tool vibration, the changeable depth of cut for the grinding wheel results in a sequence of periodic "peaks" and "troughs" on the ground surface and accumulates continuously with the machining cycles. In this case, a certain number of waviness marks around the rotating centre of the workpiece is developed, which results in regular micro waviness and determined micro-texture on the ground surface. Macro-waviness reflected macro structure of vibration mark pattern and surface texture presents micro-structure of periodical surface dimple. Due to the constant rotation speed and feed rate for the workpiece, the tool path is a spiral in X-Y plane as shown in Fig. 1(a). The micro-texture is formed by the successive overlap trajectories of tool cutting profile between the adjacent tool paths as shown in Fig. 1(b).

Figure 2 shows the surface generation geometry in ultra-precision grinding, in which the vibration of the grinding wheel with a small amplitude causes the periodical variation of ground surface profile height. It results in waviness structure generation along the radical section of the workpiece. The phase shift of tool vibration plays a significant role in the evolution of micro structure of vibration marks, especially there is an approximate rhombus texture structure formation when the phase is equal to 0.5 (second phase shift). The phase shift caused by the non-integer speed ratio of wheel and workpiece, in which there is an angle increment for surface

Optics EXPRESS

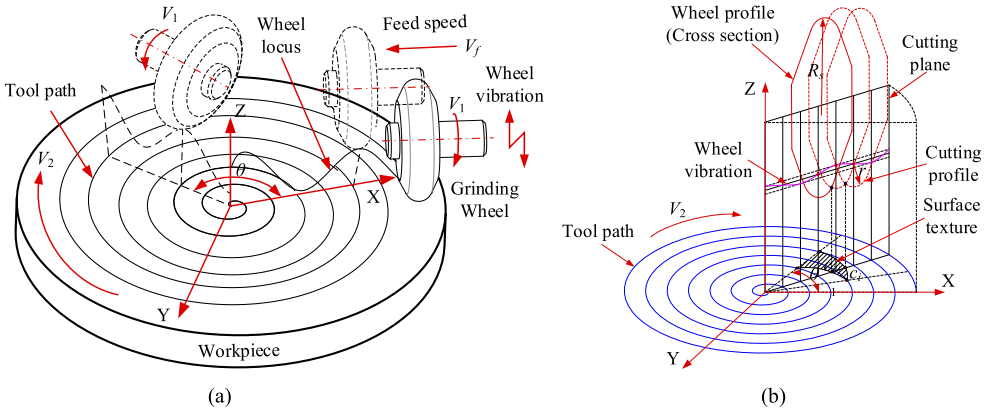

Fig. 1. Schematic representation of surface micro-texture generation mechanism (a) the relative vibration of the grinding wheel, (b) relevant surface micro-texture formation

waviness at the same angle position after the workpiece complete one cycle. In the case of phase shift difference for the tool vibration between the current and previous cutting path at the same angular position, the engagement depth of grinding wheel is different, which cause the different intersections of cutting profiles between neighboring tool paths. To simulate the deterministic micro-texture generation, the location of wheel cutting profile and the discrete points of tool trajectory with equal angle interval and feed spacing are calculated.

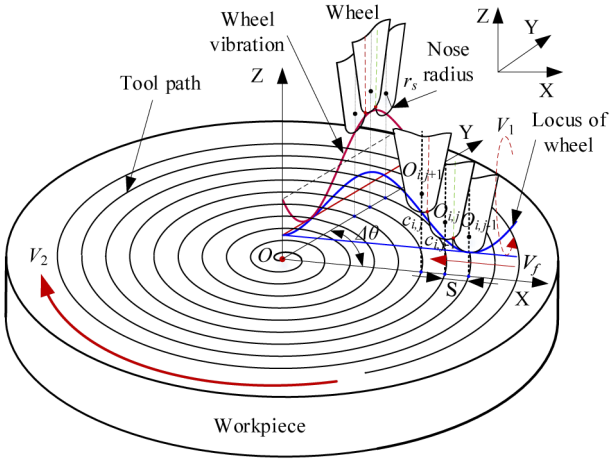

Fig. 2. Definition of micro-texture generation geometry in ultra-precision grinding with wheel vibration

In order to look insight into the micro-texture generation, an analytical model of the micro texture is developed by considering the wheel imbalanced vibration. In the workpiece coordinate system, the relative cutting point in X-Y plane can be calculated as

$$\begin{cases} \theta(i,j) = i\Delta\theta + 2\pi(j-1) \\ \rho(i,j) = R_w - \frac{\theta(i,j)SV_2}{\omega_2} \end{cases} \tag{1}$$

where $\theta(i,j)$ is angular position of grinding wheel (Rad), $\rho(i,j)$ is radial position of the grinding wheel (mm), $\Delta\theta$ is workpiece rotation Angle (Rad), and R_w is radius of workpiece (mm).

Optics EXPRESS

From Eq (1), the instant distance between the cutting point and the centre of workpiece spindle rotation is derived as

$$\rho(i,j) = R_w - \left[i + \frac{2\pi(j-1)}{\Delta\theta} \right] \frac{\Delta\theta V_f}{2\pi V_2} \tag{2}$$

where V_f is grinding wheel feed speed (mm min^{-1}) and V_2 is speed of workpiece spindle (rpm).

The grinding wheel with an oscillation movement moves along a spiral trace with respect to the workpiece, in which the vibration marks were generated by the tool cutting face, as shown in Fig. 3. As the wheel traveled along X-axis with a feed rate S, while the workpiece rotates with a revolving speed V_2. Due to the fine feed speed adopted in ultra-precision grinding, the corresponding micro-texture generation was resulted from the interference of neighboring cutting tool profiles during the machining process.

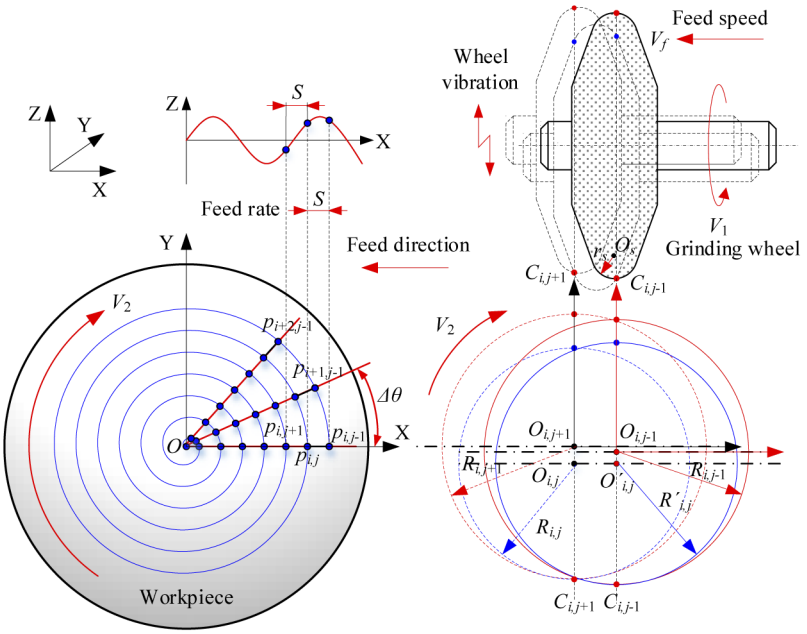

Fig. 3. Definition of coordinate systems and cutting geometry for modelling of determined micro texture generation in ultra-precision grinding

Under ideal conditions, the ground surface topography is formed by the envelopment of wheel cutting profile, in which a spiral groove with an interval (S) can be generated. However, the wheel unbalanced vibration frequently appears due to uneven tool wear, eccentricity, and runout. In this case, the depth of cut for the grinding wheel presents a periodical variation. The locus of the wheel can be approximated as a sinusoidal motion and the wheel centre with respect to the workpiece surface by considering the tool vibration can be expressed as

$$\begin{cases} x(i,j) = \left[R_w - (i-1)\frac{S}{N_1} - (j-1)S \right] \sin(i\Delta\theta), \ (i = 1,2,\ldots,N_1), \ (j = 1,2,\ldots,N_2) \\ y(i,j) = \left[R_w - (i-1)\frac{S}{N_1} - (j-1)S \right] \cos(i\Delta\theta), \ for\ N_1 = \frac{2\pi}{\Delta\theta}, N_2 = \frac{R_w}{S} \\ z(i,j) = A\sin(\frac{2\pi f_w i\Delta\theta}{\omega_1} - \varphi), \ for\ \varphi = 2\pi \left[\frac{V_1}{V_2} - INT\left(\frac{V_1}{V_2}\right) \right] \end{cases} \tag{3}$$

where S is feed rate of grinding wheel (mm r^{-1}), A is amplitude of grinding wheel vibration (mm), f_w is speed-frequency of grinding wheel (r s^{-1}), ω_1 is wheel angular velocity (rad min^{-1}), φ is vibration phase (rad), and V_1 is speed of grinding wheel spindle (rpm).

Optics EXPRESS

The determined micro-texture is formed by the enveloped cycles of successive arc cutting profile of wheel circumference as the tool moved toward the centre of workpiece with a constant feed speed, as shown in Fig. 4(a). The instantaneous surface scallop height is determined by the neighboring cutting passes, in which the different phases (phase is the angular representation of the phase shift, phase = phase shift×2π) of the tool vibration contribute to variable intersection points between adjacent wheel cutting profiles. According to the grinding wheel geometry and its associated coordinate system, the cutting profile for the grinding wheel can be calculated as

$$\begin{cases} z(x_i, y_{j-1}) = A\sin\left[\frac{2\pi f_w(i-1)\Delta\theta}{\omega_1} - \varphi\right] + \sqrt{r_s{}^2 - [x_i - (j-1)S]^2} + r_s \\ z(x_i, y_j) = A\sin\left[\frac{2\pi f_w i\Delta\theta}{\omega_1} - \varphi\right] + \sqrt{r_s{}^2 - (x_i - jS)^2} + r_s \\ z(x_i, y_{j+1}) = A\sin\left[\frac{2\pi f_w(i+1)\Delta\theta}{\omega_1} - \varphi\right] + \sqrt{r_s{}^2 - [x_i - (j+1)S]^2} + r_s \end{cases} \tag{4}$$

where r_s Nose radius of grinding wheel (mm).

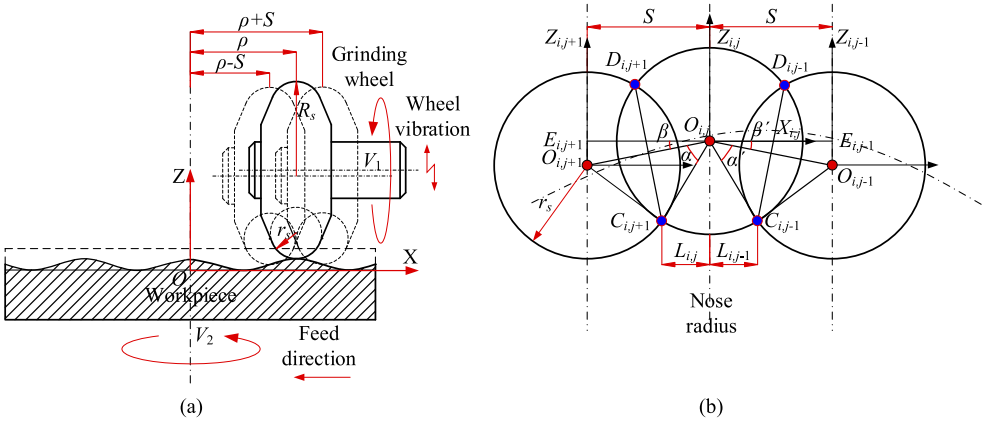

Fig. 4. Schematic diagram illustrating the surface micro-texture generation (a) interaction of the grinding wheel and workpiece, (b) determining the cutting profile interaction in ultra-precision grinding

The depth of cut for the tool cutting edge varies periodically during the wheel vibration, which also leads to the regular change for the distance between the centres of two adjacent wheel nose arcs, as shown in Fig. 4(b). The variable distance between the centres of two adjacent circles determine the micro-structure geometry and can be derived as

$$O_{i,j+1}O_{i,j} = \sqrt{(x'_{i,j} - x'_{i,j+1})^2 + (z'_{i,j} - z'_{i,j+1})^2} \tag{5}$$

The angle α can be calculated as

$$\cos\alpha = \frac{|O_{i,j+1}O_{i,j}|}{2r_s} = \frac{\sqrt{(x'_{i,j} - x'_{i,j+1})^2 + (z'_{i,j} - z'_{i,j+1})^2}}{2r_s} \tag{6}$$

$$\alpha = \arccos\left(\frac{O_{i,j+1}O_{i,j}}{2r_s}\right) = \arccos\left(\frac{\sqrt{(x'_{i,j} - x'_{i,j+1})^2 + (z'_{i,j} - z'_{i,j+1})^2}}{2r_s}\right) \tag{7}$$

Optics EXPRESS

The angle β can be calculated as

$$\beta = \arcsin\left(\left|\frac{z'_{i,j} - z'_{i,j+1}}{\sqrt{O_{i,j+1}O_{i,j}}}\right|\right) = \arcsin\left(\left|\frac{A\sin\left[\frac{2\pi f_w j\Delta\theta}{\omega_1} - \varphi\right] + \sqrt{r_s{}^2 - (x_i - jS)^2} - A\sin\left[\frac{2\pi f_w (j+1)\Delta\theta}{\omega_1} - \varphi\right] + \sqrt{r_s{}^2 - [x_i - (j+1)S]^2}}{\sqrt{(x'_{i,j} - x'_{i,j+1})^2 + (z'_{i,j} - z'_{i,j+1})^2}}\right|\right) \tag{8}$$

In a similar way, the angle α and β can be calculated as

$$\alpha' = \arccos\left(\frac{O_{i,j}O_{i,j-1}}{2r}\right) = \arccos\left(\frac{\sqrt{(x'_{i,j} - x'_{i,j-1})^2 + (z'_{i,j} - z'_{i,j-1})^2}}{2r}\right) \tag{9}$$

$$\beta' = \arcsin\left(\left|\frac{z'_{i,j} - z'_{i,j-1}}{\sqrt{O_{i,j}O_{i,j-1}}}\right|\right) = \arcsin\left(\left|\frac{A\sin\left[\frac{2\pi f_w j\Delta\theta}{\omega_1} - \varphi\right] + \sqrt{r_s{}^2 - (x_i - jS)^2} - A\sin\left[\frac{2\pi f_w (j-1)\Delta\theta}{\omega_1} - \varphi\right] + \sqrt{r_s{}^2 - [x_i - (j-1)S]^2}}{\sqrt{(x'_{i,j} - x'_{i,j-1})^2 + (z'_{i,j} - z'_{i,j-1})^2}}\right|\right) \tag{10}$$

Due to the fine feed speed adopted in the ultra-precision grinding, the interference effect between the adjacent cutting path plays a key role in the evolution of ground surface topography, especially for micro surface texture geometry generated by a tool oscillation motion during grinding. To determine the micro surface texture geometry, the point of intersection of two adjacent tool profile along the feed direction need to be solved. Based on the geometrical relationship between the wheel and workpiece as shown in Fig. 4(b), the intersection point $C_{i,j+1}$ $(x_{i,j+1}, z_{i,j+1})$ coordinate can be calculated as

$$x_{i,j} = x'_{i,j} - r_s\cos(\alpha + \beta) \tag{11}$$

$$z_{i,j} = A\sin\left[\frac{2\pi f_w j\Delta\theta}{\omega_1} - \varphi\right] + \sqrt{r_s{}^2 - (x_i - jS)^2} + r_s - r_s\sin(\alpha + \beta) \tag{12}$$

In the same way, the intersection point $C_{i,j+1}$ $(x_{i,j-1}, z_{i,j-1})$ coordinate can be derived as

$$x_{i,j-1} = x'_{i,j} + r_s\cos(\alpha' + \beta') \tag{13}$$

$$z_{i,j-1} = A\sin\left[\frac{2\pi f_w j\Delta\theta}{\omega_1} - \varphi\right] + \sqrt{r_s{}^2 - (x_i - jS)^2} + r_s - r_s\sin(\alpha' + \beta') \tag{14}$$

Since the micro-texture generation is the result of the relative motion between the workpiece and the tool, a coordinate transformation is required to conduct to transform the two coordinate systems into the same one, as shown in Fig. 5. The tool frame X'-Y'-Z' and workpiece coordinate system X''-Y''-Z'' are transformed to the fixed global frame X-Y-Z.

Optics EXPRESS

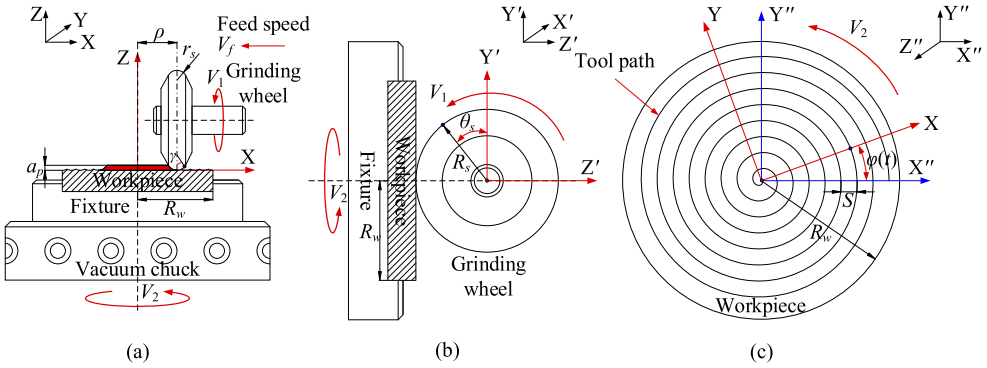

Fig. 5. Definition of the wheel-workpiece coordinate systems and the coordinate transformation in ultra-precision grinding (a) workpiece coordinate system, (b) grinding wheel coordinate system, (c) global coordinate system

The cutting point on the grinding wheel surface in the wheel coordinate system can be drived as

$$P_s(x', y', z') = \begin{bmatrix} \rho + r_s \sin(\gamma) \\ [R_s - r_s \cos(\gamma)] \cos(\omega_1 t) \\ [R_s - r_s \cos(\gamma)] \sin(\omega_1 t) \end{bmatrix} \left[-\frac{\pi}{2} \le \gamma \le \frac{\pi}{2} \right], \ [0 \le \omega_1 t \le 2\pi] \tag{15}$$

The point on the workpiece surface in the workpiece coordinate system can be drived as

$$\begin{bmatrix} x \\ y \end{bmatrix} = \begin{bmatrix} \cos(\omega_2 t) & -\sin(\omega_2 t) \\ \sin(\omega_2 t) & \cos(\omega_2 t) \end{bmatrix} \times \begin{bmatrix} x' \\ y' \end{bmatrix} \ [0 \le \omega_2 t \le 2\pi] \tag{16}$$

$$z = z' = [R_s - r_s \cos(\gamma)] \cos(\omega_1 t) \tag{17}$$

Similarly, after a coordinate transformation, the intersection point between neiguboring cutting profile in Eq. (9) and Eq. (10) can be rewritten as

$$\begin{aligned} \begin{bmatrix} \mathrm{X}_{i,j} \\ \mathrm{Y}_{i,j} \end{bmatrix} &= \begin{bmatrix} \cos(\omega_2 t) & -\sin(\omega_2 t) \\ \sin(\omega_2 t) & \cos(\omega_2 t) \end{bmatrix} \times \begin{bmatrix} x_{i,j} \\ y_{i,j} \end{bmatrix} \\ &= \begin{bmatrix} [x'_{i,j} - r_s \cos(\alpha + \beta)] \cos(\omega_2 t) - [R_s - r_s \cos(\gamma)] \cos(\omega_1 t) \sin(\omega_2 t) \\ [x'_{i,j} - r_s \cos(\alpha + \beta)] \sin(\omega_2 t) + [R_s - r_s \cos(\gamma)] \cos(\omega_1 t) \cos(\omega_2 t) \end{bmatrix} \end{aligned} \tag{18}$$

$$Z_{i,j} = z_{i,j} = A \sin\left[\frac{2\pi f_w j \Delta\theta}{\omega_1} - \varphi \right] + \sqrt{r_s{}^2 - (x_i - jS)^2} + r_s - r_s \sin(\alpha + \beta) \tag{19}$$

3. Phase shift and deterministic surface micro-texture

The deterministic micro-texture generation resulted from the regular unbalanced wheel vibration, in which the tool vibration frequency is equal to wheel rotational speed. Under the certain amplitude of wheel oscillation, the phase shift determined the relative position change between the wheel and workpiece in the cutting cycles, which caused different engagement condition and generated the different surface waviness pattern and texture unit on the ground surface. In our previous studies, it is found that the speed ratio of wheel and workpiece is the key variable to

Optics EXPRESS

determine the vibration mark geometry [17,19]. If the ratio is equal to an integer, the peaks and troughs of micro-waviness are distributed on the same angular section, and the surface microwave texture presents a linear distribution. In this case, no phase shift occurs However, if the ratio is not an integer, there is an angle increment in each successive revolution for the micro-waviness, which results in the staggered arrangement of microwave marks, as shown in Fig. 6. In general, the number of the microwaviness is equal to the ratio of the grinding wheel speed to the workpiece speed. However, the number of microwave lines is twice the integer part of speed ratio of grinding wheel to workpiece when the phase shift is equal to 0.5, in which every another grinding pass, the engagement depth phase coincides with the current one at the same angular position in the grinding cycles. In this case, the second phase shift plays a major role in the formation of the deterministic surface texture. It is called the second phase shift in this paper, as shown in Fig. 6(b). It indicates that there are two phase mechanisms involved in the determined micro-waviness generation.

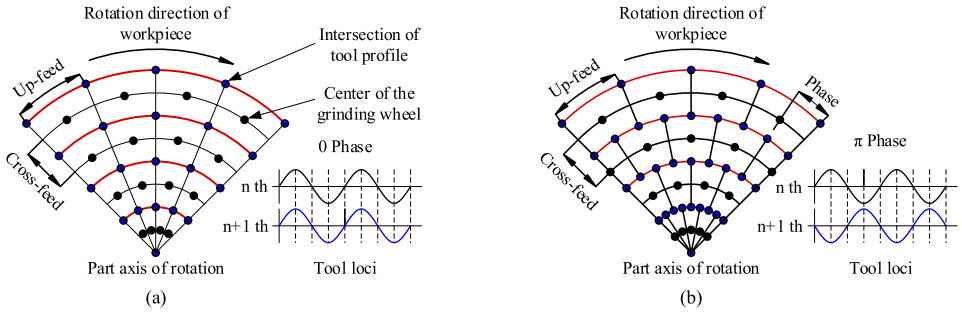

Fig. 6. Illustration of phase shift effects on surface generation (a) phase shift = 0, (b) phase shift = 0.5

Under ideal conditions, if the grinding wheel speed is an integer multiple of the workpiece, the surface ripples are located in the same radial position and arranged in straight line mode without phase shift, as shown in Fig. 7(a). When there is a small phase shift, for example, when the phase shift is 0.1, the straight microwave texture turns into a curve, as shown in Fig. 7(b). For the primary phase shift, a slight difference for the phase between the neighboring cutting passes at the same angular position and the number of waviness marks is equal to the integral part of the speed ratio of wheel and workpiece. It results in continuous waviness shift under grinding cycles and generates a series of deterministic waviness on the ground surface. However, for the second phase shift, when the grinding wheel speed is equal to an integer multiple plus half of the workpiece speed (i.e., the phase shift is 0.5), the micro-waviness marks on every two feed intervals are arranged in a straight mode, as shown in Fig. 7(c).

In this case, there are large phase difference between the adjacent tool paths, in which the same phase coincides with every two cutter pathes and the number of vibration marks is double to the integral part of the speed ratio of tool and workpiece. Similarly, when the micro-phase shift based on the second phase shift (i.e. the phase shift is 0.51), the linear texture of the second phase shift becomes the curved texture distribution, and the curve geometry is the same as that of the primary micro-phase shift, as shown in Fig. 7(d). In reality, there is little possibility for coinciding with an integer speed ratio between the wheel and workpiece due to the small rotation error of grinding wheel in the high-speed grinding, thus phase shift is almost impossible to be eliminated. In this case, the small fractional part of the ratio will produce incremental phase shift for each cycle, which results in the evolution and accumulation of micro-microwave (curve pattern) instead of the straight line pattern. A high-precision vibration sensor (Brüel & Kjaer Vibro-Vibrotest 60) was used to measure the actual rotational speed of grinding wheel, in which

Optics EXPRESS

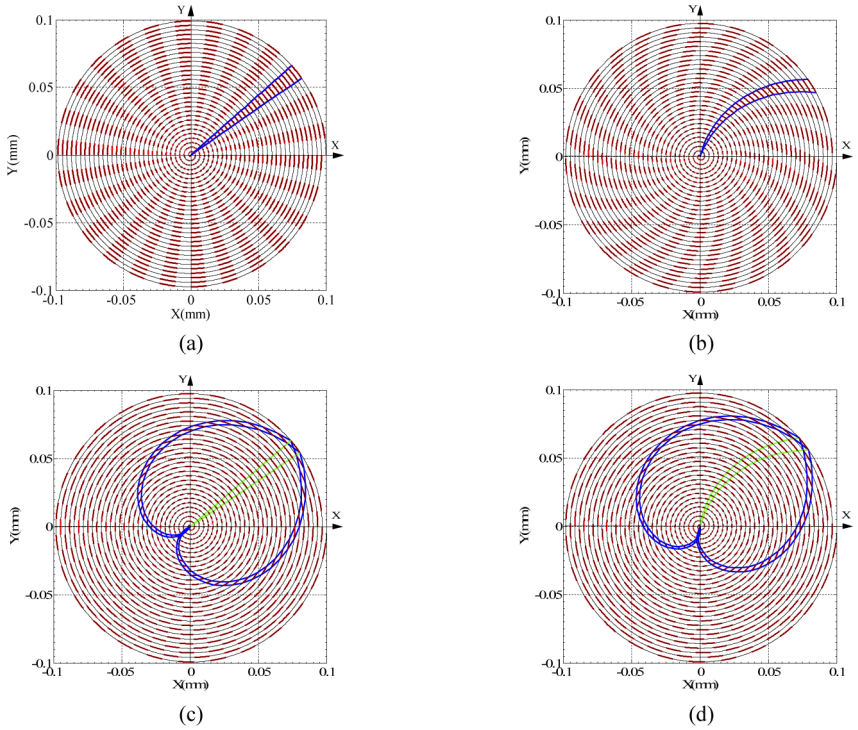

Fig. 7. Illustration of double phase shift mechanisms for surface generation with $V_2 = 1500$ rpm, $V_f = 10$ mm/min (a) phase shift = 0 ($V_1 = 39000$ rpm), (b) small phase shift = 0.1 ($V_1 = 39150$ rpm), (c) phase shift = 0.5 ($V_1 = 39750$ rpm), (d) small second phase shift = 0.51 ($V_1 = 39765$ rpm). Blue and green lines represent the primary and second phase shift marks respectively

20 speed values were recorded and got the average. It is found that the actual wheel spindle speed was about 22 rpm faster than the setting speed for all speed range.

4. Experimental setup

The experiments were carried out on a Moore Nanotech ultra-precision CNC 4-axis grinding machine (450UPL), which is consisted of two hydrostatic slides in X-Z configuration with two air bearing spindles and it is suitable for both single-point diamond turning and grinding. It is capable to reach the surface roughness at the sub-nanometer scale and form error at the sub-micron. The grinding wheel spindle is mounted on a rotary table (B axis) and the workpiece spindle rotates and feeds along X axis to realize the whole surface machining, as shown in Fig. 8. The wheel and workpiece specifications are summarized in Table 1. To realize the adjustment of phase shift in the grinding test, the workpiece spindle speed is fixed at 1500 rpm and the wheel rotation speed ranged from 39150 rpm to 40500 rpm (adjust the wheel speed to make the speed ratio generate the expected value). In grinding, tool wear has a considerable impact on micro-texture generation both for texture unit shape and surface finish. To reduce the effect of grinding wheel wear on surface generation, all workpieces are ground by using a fine grinding wheel to get a high-quality flat surface, then doing the tests and conducting fine dressing before each test. An ultra-high speed laser displacement sensor (KEYENCE LK-G5000 Series) is mounted to the B axis of the grinding machine to measure the vibration amplitudes of grinding wheel. The resolution

Optics EXPRESS

and sampling frequency of the laser displacement sensor are 0.1μm and 50 KHz respectively in measurement process. To measure the surface micro-texture for the vilification of the developed model, a 3D optical coherence scanning interferometric profiler (Nexview NX2) is used after grinding tests.

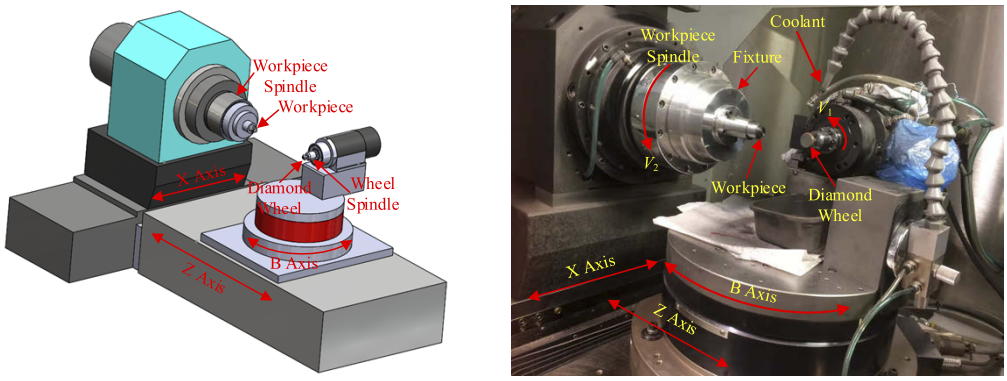

(a) (b)

Fig. 8. Schematic diagram of Moore Nanotech 450UPL grinding machine (a) the outline of the 4-axis grinding machine tool, (b) overview of the experimental setup

Table 1. Grinding wheel and experimental conditions

Contents	Condition
Grinding wheel type	Resin bond CBN wheel
Wheel size	Diameter: 20 mm, thickness: 5 mm
Grain size	#1500
Nose radius	0.5 mm
Workpiece	Mold Steel
Cooling fluid	CLAIRSOL 330

5. Experimental validation

In order to validate the theoretical analysis of phase shift involved in the micro-waviness generation in the grinding, the phase shift set of grinding tests was conducted in the CNC 4-axis grinding machine. The phase shift was controlled by adjusting the wheel speed, in which the workpiece speed was set at 1500 rpm and made the speed ratio generate expected value. Figure 9 shows a comparison of the primary and second phase shift experimental results. For the primary phase shift (0.1), it resulted in the evolution and accumulation of surface micro-waviness and eventually it transforms into the continuous spiral marks around the rotation centre of workpiece in the grinding cycles and the corresponding texture is the continuous grooves left by the grinding wheel cutting profile. However, for the second phase shift (0.5), surface micro-waviness has the form of discontinued spiral marks, in which there is a huge difference for the depth of cut of tool engagement and results in discontinuous texture unit and the tool vibration phase happens to be the same every two tool paths. The experiment results indicated that the phase mechanism of deterministic micro-waviness agrees reasonably well with previous theoretical analyses.

It is noticed that the vibration associated with the unbalanced wheel posed a uniformly radical distribution of spiral marks around the centre of workpiece and the number of spirals is equal

Optics EXPRESS

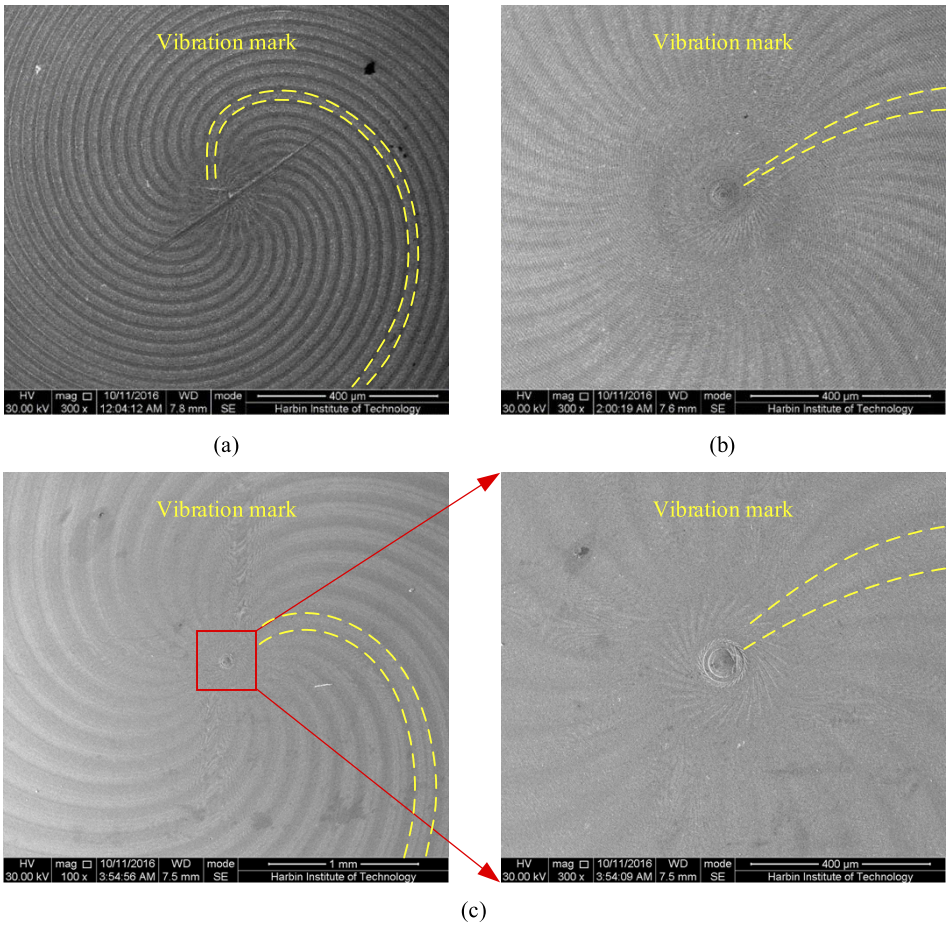

Fig. 9. SEM images for the micro vibration marks with $V_2 = 1500$ rpm, $V_f = 10$ mm/min, depth of cut $a_p = 10$ μm, (a) phase shift = 0.1 ($V_1 = 39150$ rpm), (b) phase shift = 0.5 ($V_1 = 39750$ rpm), (c) phase shift = 1 (0) ($V_1 = 40500$ rpm)

to the integer portion of speed ratio between the rotational speed of the grinding wheel and workpiece. For example, the number is 26 ($V_1/V_2 = 39150/1500 = 26.1$) as shown in Fig. 9(a). However, the number of spirals is double to the speed ratio, e.g. 53 ($2V_1/V_2 = 2\times39750/1500 = 53$) as shown in Fig. 9(b). At the same time, the second phase shift predominated role in the evolution of determined vibration marks, which is originated from the finer cross-feed rate than the up-feed rate. In this condition, the second phase shift occurred and govern the surface generation. The number of spirals is equal to 27 ($V_1/V_2 = 40500/1500 = 27$) and it is found that the spiral shape is almost the same for two different phase shifts (the phase shift 0.5 and phase shift 0), as shown in Fig. 9(c). The amplitude of wheel vibration measured by the laser displacement sensor is about 2.5 μm. By recording the actual wheel speed values, it is found that the operational wheel speed is nearly 20 rpm higher than the set value under different phase shifts, thus the micro-waviness presents a curved striation pattern, which agrees with the theoretical analysis well (as shown in Fig. 7).

In addition to generating a series of determined micro-waviness, the phase shift also results in determined micro-texture generation on the ground surface due to the regular superposition of tool vibration at a determined frequency, in which the wheel engaged into the workpiece

Optics EXPRESS

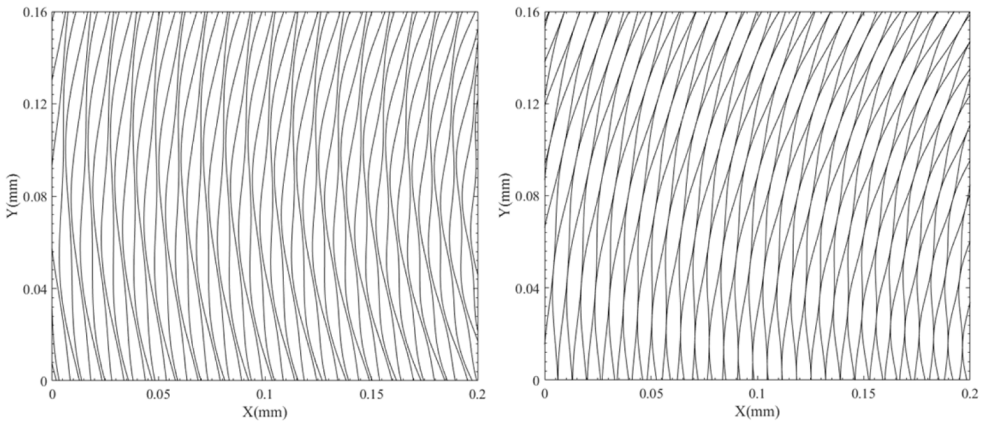

Fig. 10. Simulated deterministic surface micro-texture with $V_2 = 1500$ rpm, $V_f = 10$ mm/min (a) phase shift = 0.3 ($V_1 = 39450$ rpm), (b) phase shift =0.5 ($V_1 = 39750$ rpm)

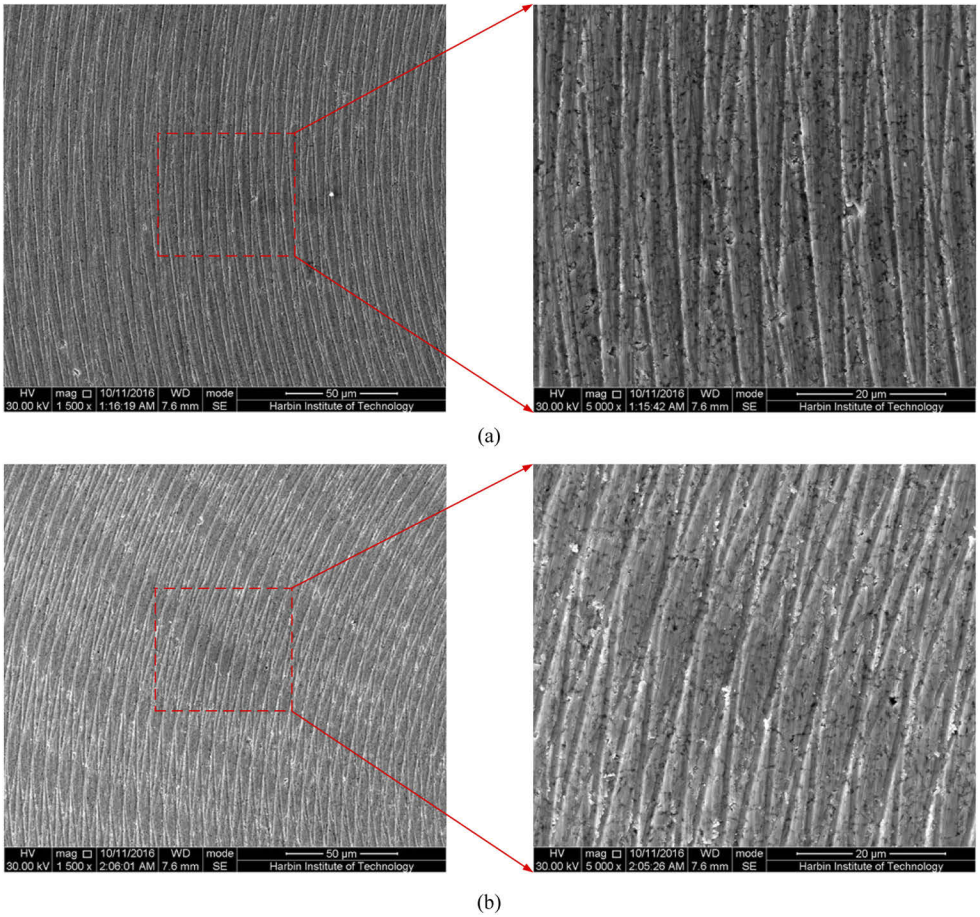

Fig. 11. SEM images for the micro surface texture with $V_2 = 1500$ rpm, $V_f = 10$ mm/min, depth of cut $a_p = 10$ μm (a) phase shift = 0.3 ($V_1 = 39450$ rpm), (b) phase shift =0.5 ($V_1 = 39750$ rpm)

Optics EXPRESS

with a continuously varying depth of cut. Under different phase shifts, the relative interference position of wheel cutting profile between neighboring cutting paths altered with machining cycles, which resulted in the determined micro-texture on the machined surface. Especially, there is an approximate rhombus-shaped surface texture generated due to the same vibration phase of the grinding wheel every two intervals for the tool path when the phase shift is equal to 0.5 (second phase shift), as shown in Fig. 10(b). Figure 11 shows SEM images of micro-texture structure on the machined surface when the phase is equal to 0.3 and 0.5 respectively and it is found that the radical rhombus-shaped texture was visible on the ground surface, which agrees well with the measured surface. It indicates the model proposed in this research is capable of accurately predicting the surface micro-texture generation.

From the discussion relating to deterministic surface micro-texture formation in the grinding, it is clear that the phase shift is capable of generating micro-texture surface by controlling the phase between the tool oscillation and workpiece rational frequency, in particular, the phase shift is equal to 0.5 and the second phase shift acted the dominated wave marks. This makes it feasible to generate regular surface texture by the way of adjusting the phase shift. The phase shift changed by adjusting the ratio of the tool oscillation frequency to rotational frequency so as to produce non-integral ratio. For example, the oscillation frequency is 150 times per minute and the workpiece rotational speed is 20 rpm, the speed ratio is calculated as 150/20 = 7.5, the phase

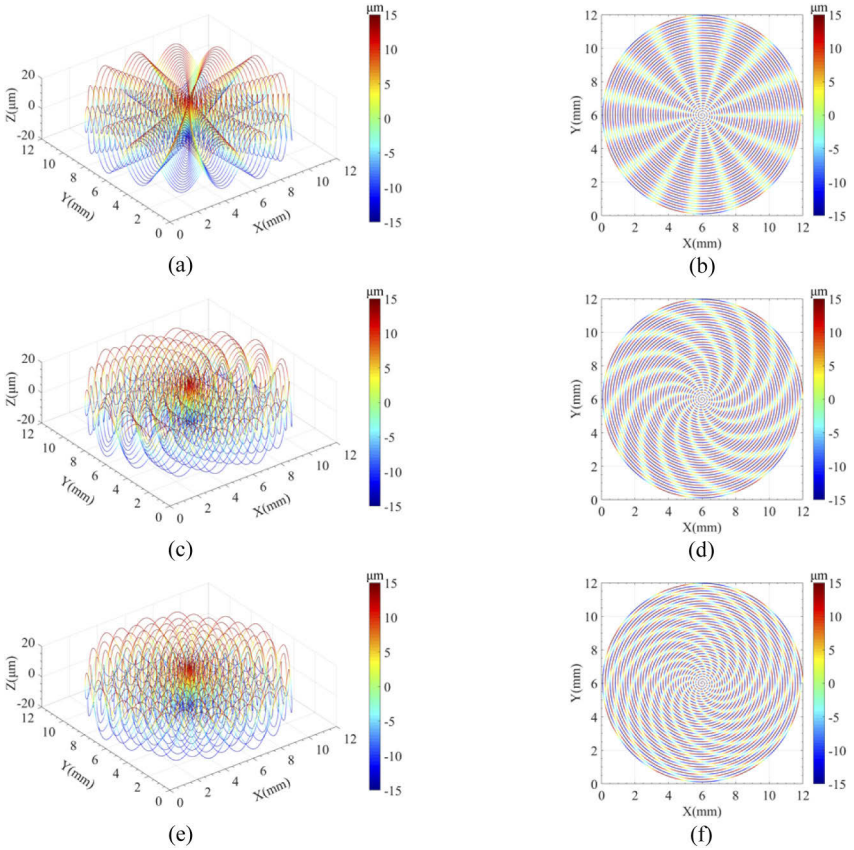

Fig. 12. Tool path generation of phase control for grinding of the deterministic surface micro-texture: (a),(c),(e) 3D tool path (phase shift = 0.5, 0.55 and 0.6 respectively) and (b),(d),(f) corresponding tool path projection in X-Y plane

Optics EXPRESS

shift is 0.5. Based on the previous discussion, a novel tool path planning strategy to control the phase between the workpiece spindle speed-frequency and sinusoidal oscillation along the Z axis direction is presented.

In order to change the phase shift, the workpiece spindle speed, wheel oscillation amplitude, and feed speed are kept at 20 rpm, 15 μm and 1 mm/min respectively and the oscillation frequency is set at 150,151 and 152 times per minute, in which the phase shift is equal to 0.5,0.55 and 0.6 respectively, as shown in Fig. 12. It is observed that the number of wave structure pattern is twice the ratio of tool oscillation frequency to workpiece speed frequency. The pattern of wave structure presents a radical linear distribution when the ratio is 7.5 and there is a curved distribution for the wave structure for the tool path despite a small change for the ratio, which consistent with the previous analysis.

It is indicated that the number of micro-structure striation is of twice the integral part of the ratio between the oscillation frequency and workpiece speed (the number of radial striations is equal to 15 for the phase shift = 0.5,0.55,0.6) and it has a straight mode distribution for the texture pattern when the phase is 0.5 as shown in Fig. 12(a) and Fig. 12(b), which is consistent with the

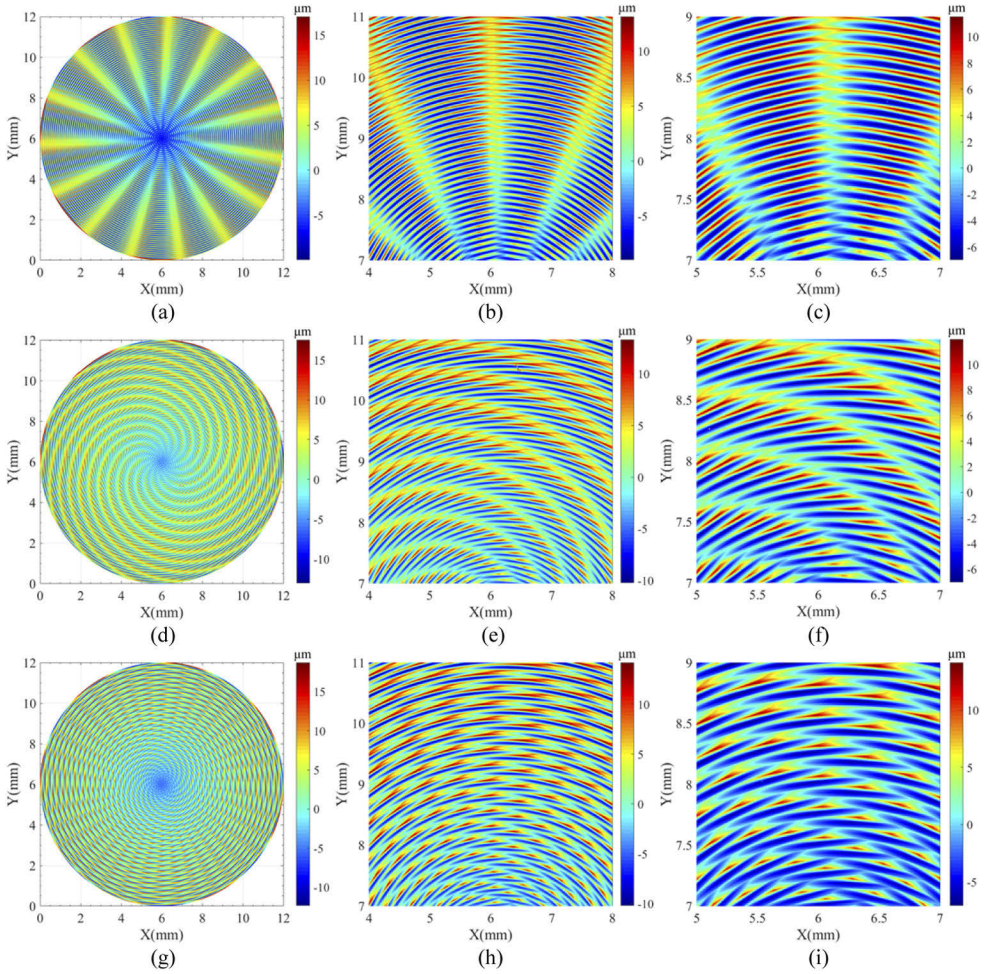

Fig. 13. 3D maps for the surface micro-texture (a),(b),(c) phase shift = 0.5, (d),(e),(f) phase shift = 0.55, (g),(h),(i) phase shift = 0.6

Optics EXPRESS

previous analysis. However, there is a significant change for the texture pattern in spite of a slight change for the oscillation frequency, in which the texture pattern is changed into the radial curved striation as shown in Fig. 12(c)–12(f). It indicates that the phase shift acts a significant role in the deterministic micro-structure generation, which offers an alternative approach of fabricating micro-structure surface by controlling the phase shift.

An ultra-precision optical profiling system is used to measure the 3D topography of the ground surface. It is found that the rhombus-shaped micro-structure has been formed, which embraces a radial straight distribution for micro-structure pattern around the workpiece centre in the case of phase shift 0.5 as shown in Fig. 13(a)–13(c). In addition, the straight-line mode for texture generation is changed into a curve pattern when a small change for the phase shift and the approximate rhombus-shaped and regular triangular ridge texture are generated, as shown in Fig. 13(d)–13(f) and Fig. 13(g)–13(i). There is an angle increase along circumferential direction for the second phase of micro-waviness as a slight change for the phase shift (from 0.5 to 0.55), which cumulates in the following grinding cycles and it finally evolves into a curved arrangement of micro-structure pattern. It is observed that the relative length of the micro-structure unit decreased with the grinding wheel moves from the outer to the centre of workpiece, which is caused by the decreasing linear velocity (constant workpiece spindle speed). It is found that the micro-structure unit and its distribution pattern are extremely regular in a large area and the width of rhombus-structure is approximately equal to two feed rate spacing, which agree with the previous analysis well. It indicates that the new proposed tool path for phase shift control can be used to fabricate the deterministic surface micro-structure both for the pattern mode and various shapes. The phase control has a flexibly tunable feature of deterministic surface micro-structure, which could be a new access to fabricate different kinds of textural surface effectively in the grinding.

6. Conclusion

The deterministic surface micro-texture generation mechanism is studied theoretically and experimentally, which resulted from the unbalanced vibration of an arc grinding wheel. Based on the resulted surface texture analysis, a novel tool path planning for phase control in the ultra-precision grinding is proposed, which can be exploited for the fabrication of flexibly tunable features of deterministic surface texture. Conclusions from this research can be summarized as follows:

(1) There are primarily two types of deterministic surface textural pattern involved in the ground surface generation. The primary phase shift related to the speed ratio between the rotational speed of grinding wheel and workpiece determines the number of the vibration waviness and pattern geometry on the ground surface. However, the second phase shift embraces the same waviness pattern geometry with the primary phase = 0, in which the waviness marks are generated in an interval regard to the cross-feed distance space and the number of the marks is equal to twice of the speed ratio.

(2) The second phase shift dominates the deterministic textural pattern generation when the phase shift is 0.5 and results in deterministic rhombus-shaped texture generation resulted from the neighboring interference of grinding passes, in which, the oscillation phase is consistent for every two intervals in the same angular position.

(3) The slight change for the phase shift can contribute to a significant effect both for the textural pattern and micro-structure, which leads to phase cumulates in the grinding cycles and it finally evolves into very different arrangements of micro-texture pattern and texture unit. It indicates the phase shift has a major influence on the micro-texture generation in ultra-precision grinding.

Optics EXPRESS

(4) By combining tool oscillation motion and phase control, the rhombus-shaped microstructure was generated and more complex deterministic textures can be fabricated by a small adjustment for the phase shift.

Funding. National Natural Science Foundation of China (52105481); China Postdoctoral Science Foundation (2019M663681); Natural Science Foundation of Zhejiang Province (LQ21E050010); Scientific Research and development plan for Beilin District (Xi'an city, Shaanxi Province) 2020 (GX2028); China Scholarship Council (202006285057); PhD studentship from Hong Kong Polytechnic University (RU3K).

Disclosures. The authors declare no conflicts of interest.

Data availability. Data underlying the results represented in this paper are not publicly available at this time but may be obtained from the authors upon reasonable request.

References

1. Z. Y. Zhang, J. W. Yan, and T. Kuriyagawa, "Manufacturing technologies toward extreme precision," Int. J. Extrem. Manuf. **1**(2), 022001 (2019).
2. S. J. Zhang, Y. P. Zhou, H. J. Zhang, Z. W. Xiong, and S. To, "Advances in ultra-precision machining of micro-structured functional surfaces and their typical applications," International Journal of Machine Tools and Manufacture **142**, 16–41 (2019).
3. G. J. Ding, R. J. He, K. Q. Zhang, N. P. Zhou, and H. Xu, "Stereolithography 3D printing of SiC ceramic with potential for lightweight optical mirror," Ceram. Int. **46**(11), 18785–18790 (2020).
4. Y. Zhang, Q. Wang, C. Li, Y. C. Piao, N. Hou, and K. N. Hu, "Characterization of surface and subsurface defects induced by abrasive machining of optical crystals using grazing incidence X-ray diffraction and molecular dynamics," J. Adv. Res. **36**, 51–61 (2022).
5. C. Li, Y. Q. Wu, X. L. Li, L. J. Ma, F. H. Zhang, and H. Huang, "Deformation characteristics and surface generation modelling of crack-free grinding of GGG single crystals," J. Mater. Process. Technol. **279**, 116577 (2020).
6. K. Hamouda, H. Bournine, M. A. Tamarkin, A. P. Babichev, D. Saidi, and H. E. Amrou, "Effect of the velocity of rotation in the process of vibration grinding on the surface state," Mater. Sci. **52**(2), 216–221 (2016).
7. I. Inasaki, B. Karpuschewski, and H. S. Lee, "Grinding Chatter – Origin and Suppression," CIRP Ann. **50**(2), 515–534 (2001).
8. Y. Liu, X. F. Wang, J. Lin, and X. G. Kong, "An adaptive grinding chatter detection method considering the chatter frequency shift characteristic," Mechanical Systems and Signal Processing **142**, 106672 (2020).
9. R. Thomazella, W. N. Lopes, P. R. Aguiar, F. A. Alexandre, A. A. Fiocchi, and E. C. Bianchi, "Digital signal processing for self-vibration monitoring in grinding: A new approach based on the time-frequency analysis of vibration signals," Measurement **145**, 71–83 (2019).
10. W. G. Mao, C. L. Hu, J. H. Li, Z. H. Huang, and G. P. Liu, "Eccentricity parameters identification for a motorized spindle system based on improved maximum likelihood method," Shock and Vibration **2020**, 1–10 (2020).
11. J. B. Chen, Q. H. Fang, and P. Li, "Effect of grinding wheel spindle vibration on surface roughness and subsurface damage in brittle material grinding," International Journal of Machine Tools and Manufacture **91**, 12–23 (2015).
12. T. Kuriyagawa, N. Yosihara, Y. B. Wu, and K. Syoji, "Formation of vertical striped pattern on the ground surface in high-reciprocation profile grinding," Journal of the Japan Society for Precision Engineering **67**(8), 1316–1320 (2001).
13. B. Chen, L. Luo, H. W. Jiao, S. S. Li, S. C. Li, Z. H. Deng, and H. H. Yao, "Affecting factors, optimization, and suppression of grinding marks: a review," Int J Adv Manuf Technol **115**(1-2), 1–29 (2021).
14. N. Zhang, I. Kirpitchenko, and D. K. Liu, "Dynamic model of the grinding process," Sound Vibration **280**(1-2), 425–432 (2005).
15. J. Badger, S. Murphy, and G. O'Donnell, "The effect of wheel eccentricity and run-out on grinding forces, waviness, wheel wear and chatter," International Journal of Machine Tools and Manufacture **51**(10-11), 766–774 (2011).
16. B. Chen, S. C. Li, Z. H. Deng, B. Guo, and Q. L. Zhao, "Grinding marks on ultra-precision grinding spherical and aspheric surfaces," Int. J. of Precis. Eng. and Manuf.-Green Tech. **4**(4), 419–429 (2017).
17. S. S. Chen, C. F. Cheung, F. H. Zhang, and C. Y. Zhao, "Three-dimensional modelling and simulation of vibration marks on surface generation in ultra-precision grinding," Precis. Eng. **53**, 221–235 (2018).
18. Y. C. Pan, Q. L. Zhao, B. Guo, B. Chen, and J. H. Wang, "Suppression of surface waviness error of fresnel micro-structured mold by using non-integer rotation speed ratio in parallel grinding process," Micromachines **11**(7), 652 (2020).
19. S. S. Chen, C. F. Cheung, and F. H. Zhang, "An experimental and theoretical analysis of surface generation in the ultra-precision grinding of hard and brittle materials," Int J Adv Manuf Technol **97**(5-8), 2715–2729 (2018).
20. S. S. Chen, S. M. Yang, Z. R. Liao, C. F. Cheung, Z. D. Jiang, and F. H. Zhang, "Curvature effect on surface topography and uniform scallop height control in normal grinding of optical curved surface considering wheel vibration," Opt. Express **29**(6), 8041–8063 (2021).
21. T. Z. Wang, H. N. Liu, C. Y. Wu, J. Cheng, and M. J. Chen, "Three-dimensional modeling and theoretical investigation of grinding marks on the surface in small ball-end diamond wheel grinding," Int. J. Mech. Sci. **173**, 105467 (2020).

Optics EXPRESS

22. Z. J. Wang, X. C. Luo, H. T. Liu, W. L. Chang, L. Yang, J. G. Zhang, and A. Cox, "A high-frequency non-resonant elliptical vibration-assisted cutting device for diamond turning microstructured surfaces," Int J Adv Manuf Technol **112**(11-12), 3247–3261 (2021).
23. Y. T. Xing, Y. Liu, C. Li, C. Yang, and C. X. Xue, "Ductile-brittle coupled cutting of a single-crystal silicon by ultrasonic assisted diamond turning," Opt. Express **29**(15), 23847–23863 (2021).
24. Z. W. Zhu, S. To, W. L. Zhu, P. Huang, and X. Q. Zhou, "Cutting forces in fast/slow tool servo diamond turning of micro-structured surfaces," International Journal of Machine Tools and Manufacture **136**, 62–75 (2019).
25. G. Li, B. Wang, J. D. Xue, D. Qu, and P. Zhang, ""Development of vibration-assisted micro-milling device and effect of vibration parameters on surface quality and exit-burr," Proceedings of the Institution of Mechanical Engineers," Part B: Journal of Engineering Manufacture **233**(6), 1723–1729 (2019).
26. S. Greco, K. Klauer, B. Kirsch, and J. C. Aurich, "Vibration-assisted micro milling of AISI 316L produced by laser-based powder bed fusion," Journal of Manufacturing Processes **71**, 298–305 (2021).
27. Y. Peng, Z. Liang, Y. Wu, Y. Guo, and C. Wang, "Characteristics of chip generation by vertical elliptic ultrasonic vibration-assisted grinding of brittle materials," Int J Adv Manuf Technol **62**(5-8), 563–568 (2012).
28. K. Wegener, F. Bleicher, P. Krajnik, H. W. Hoffmeister, and C. Brecher, "Recent developments in grinding machines," CIRP Ann. **66**(2), 779–802 (2017).
29. P. Beiring and J. W. Yan, ""Ultrasonic vibration-assisted microgrinding of glassy carbon," Proceedings of the Institution of Mechanical Engineers," Part C: Journal of Mechanical Engineering Science **233**(12), 4165–4175 (2019).
30. Z. C. Yang, L. D. Zhu, G. X. Zhang, C. B. Ni, and B. Lin, "Review of ultrasonic vibration-assisted machining in advanced materials," International Journal of Machine Tools and Manufacture **156**, 103594 (2020).
31. W. Q. Chen, D. H. Huo, Y. L. Shi, and J. M. Hale, "State-of-the-art review on vibration-assisted milling: principle, system design, and application," Int J Adv Manuf Technol **97**(5-8), 2033–2049 (2018).
32. S. L. Xu, T. Kuriyagawa, K. Shimada, and M. Mizutani, "Recent advances in ultrasonic-assisted machining for the fabrication of micro/nano-textured surfaces," Front. Mech. Eng. **12**(1), 33–45 (2017).
33. Y. H. Wang, Z. Q. Liang, W. X. Zhao, X. B. Wang, and H. Wang, "Effect of ultrasonic elliptical vibration assistance on the surface layer defect of M-plane sapphire in microcutting," Mater. Des. **192**, 108755 (2020).
34. Y. Wang, B. Lin, S. L. Wang, and X. Y. Cao, "Study on the system matching of ultrasonic vibration assisted grinding for hard and brittle materials processing," International Journal of Machine Tools and Manufacture **77**, 66–73 (2014).
35. J. P. Qiao, M. Feng, H. Q. Wu, S. S. Li, J. Zeng, and Y. B. Wu, "Experimental study on the effect of grinding path in tangential ultrasonic-assisted grinding for the curved surfaces of zirconia ceramics," Int J Adv Manuf Technol **118**(5-6), 1859–1872 (2022).
36. B. Guo and Q. L. Zhao, "Ultrasonic vibration assisted grinding of hard and brittle linear micro-structured surfaces," Precis. Eng. **48**, 98–106 (2017).
37. J. L. Jiang, S. F. Sun, D. X. Wang, Y. Yang, and X. F. Liu, "Surface texture formation mechanism based on the ultrasonic vibration-assisted grinding process," International Journal of Machine Tools and Manufacture **156**, 103595 (2020).
38. J. Khodaii, H. Adibi, F. Barazandeh, M. Rezaei, and A. A. D. Sarhan, "Investigation of the surface integrity, flexural strength on the grinding of alumina for biomedical applications," Precis. Eng. **67**, 110–122 (2021).
39. M. D. Luo, J. W. Zhao, Y. L. Ding, W. P. Miao, H. Bao, and Y. H. Zhang, "Effect of abrasive mass fraction on grinding performance of diamond grinding wheel for grinding silicon wafer," Diamond & Abrasives Engineering **41**(06), 80–84 (2021).
40. B. Lin, J. P. Zhang, Z. C. Cao, J. N. Zhou, and T. Huang, "Theoretical and experimental investigation on surface generation and subsurface damage in fixed abrasive lapping of optical glass," Int. J. Mech. Sci. **215**, 106941 (2022).
41. W. Gao, Y. X. Zhang, and P. J. Huang, "Study on material removal mechanism of 6H-SiC single crystal wafer based on different nano-scratch order," Diamond & Abrasives Engineering **41**(04), 92–97 (2021).
42. C. Li, Y. C. Piao, B. B. Meng, Y. X. Hu, L. Q. Li, and F. H. Zhang, "Phase transition and plastic deformation mechanisms induced by self-rotating grinding of GaN single crystals," International Journal of Machine Tools and Manufacture **172**, 103827 (2022).
43. Q. Liu, Z. R. Liao, and D. Axinte, "Temperature effect on the material removal mechanism of soft-brittle crystals at nano/micron scale," International Journal of Machine Tools and Manufacture **159**, 103620 (2020).